![turnitin logo]

Digital Receipt

This receipt acknowledges that Turnitin received your paper. Below you will find the receipt information regarding your submission.

The first page of your submissions is displayed below.

Submission author: Faizal Kasim

Assignment title: Cek FayKas

Submission title: 29. Physical assessment of coastal vulnerability-Faizal et al fi…

File name: sical_assessment_of_coastal_vulnerability-Faizal_et_al_final.p…

File size: 6.19M

Page count: 21

Word count: 13,420

Character count: 69,396

Submission date: 14-Nov-2021 08:09AM (UTC-0800)

Submission ID: 1702249362

29. Physical assessment of coastal vulnerability-Faizal et al final

by Faizal Kasim

Physical assessment of coastal vulnerability under enhanced land subsidence in Semarang, Indonesia, using multi-sensor satellite data

Husnayaen [a], A. Besse Rimba [a,*], Takahiro Osawa [a,f,g], I Nyoman Sudi Parwata [b], Abd. Rahman As-syakur [a,c], Faizal Kasim [d], Ida Ayu Astarini [e]

[a] *Center for Remote Sensing and Ocean Sciences (CReSOS), Udayana University, PB Sudirman Street, Denpasar, Bali 80232, Indonesia*
[b] *Graduate School of Science and Technology for Innovation, Yamaguchi University, 2-16-1 Tokiwadai, Ube 755-8611, Japan*
[c] *Marine Science Department, Faculty of Marine and Fisheries, Udayana University, Bukit Jimbaran, Bali 80361, Indonesia*
[d] *Department of Aquatic Resources Management, Gorontalo State University, Jambura Campus, Gorontalo 96128, Indonesia*
[e] *Biology Department, Faculty of Mathematics and Natural Sciences, Udayana University, Bukit Jimbaran, Bali 80361, Indonesia*
[f] *Center for Research and Application of Satellite Remote Sensing(CRAS), Yamaguchi University, 2-6-1 Tokiwadai Ube, Yamaguchi 7558611, Japan*
[g] *Regional Satellite Applications Center for Disaster Management (RSCD), Japan Aerospace Exploration Agency (JAXA), 4-1-1 Industrial Technology Institute Asutopia, Ube, Yamaguchi 7550195, Japan*

Abstract

Research has been conducted in Semarang, Indonesia, to assess coastal vulnerability under enhanced land subsidence using multi-sensor satellite data, including the Advanced Land Observing Satellite (ALOS) Phased Array type L-band SAR (PALSAR), Landsat TM, IKONOS, and TOPEX/Poseidon. A coastal vulnerability index (CVI) was constructed to estimate the level of vulnerability of a coastline approximately 48.68 km in length using seven physical variables, namely, land subsidence, relative sea level change, coastal geomorphology, coastal slope, shoreline change, mean tidal range, and significant wave height. A comparison was also performed between a CVI calculated using seven parameters and a CVI using six parameters, the latter of which excludes the land subsidence parameter, to determine the effects of land subsidence during the coastal vulnerability assessment. This study showed that the accuracy of coastal vulnerability was increased 40% by adding the land subsidence factor (i.e., CVI 6 parameters = 53%, CVI 7 parameters = 93%). Moreover, Kappa coefficient indicated very good agreement (0.90) for CVI 7 parameters and fair agreement (0.3) for CVI 6 parameters. The results indicate that the area of very high vulnerability increased by 7% when land subsidence was added. Hence, using the CVI calculation including land subsidence parameters, the very high vulnerability area is determined to be 20% of the total coastline or 9.7 km of the total 48.7 km of coastline. This study proved that land subsidence has significant influence on coastal vulnerability in Semarang.
© 2018 COSPAR. Published by Elsevier Ltd. All rights reserved.

Keywords: CVI; Semarang; Land subsidence; Remote sensing

1. Introduction

Coastal zones are dynamic and complex areas with multi-purpose uses, which often conflict with human socioeconomic activities (Turner et al., 2004). Coastal communities are usually distributed in lowland geographic ele-

vations and link with a developed area and have greater population densities than inland communities (Balica et al., 2012). In fact, most of the megacities in Asia and around the world are in coastal regions (Nicholls, 1995; Yeung, 2001), which could indicate that the population in the coastal region is vast and steadily increasing through migration (McGranahan et al., 2007). Therefore, the coastal zone is significant due to the ever-increasing number of people who live there. However, the coast is one of the areas that is most vulnerable to the potential impacts of natural and anthropogenic hazards, primarily due to the impacts of climate change and human activities, which lead to future sea level rise and land subsidence (Abidin et al., 2013; Nguyen et al., 2016). Physical processes such as tidal inundation, sea level rise, land subsidence, and erosion-sedimentation have an essential role in coastal landscape development (Marfai & King, 2008). Land subsidence and sea level rise (SLR) will result in the permanent flooding of low-lying areas, inland extension of episodic flooding, increased beach erosion, and saline intrusion (Cooper & Beevers, 2008; Wang et al., 2012).

Indonesia is the largest archipelagic country and has the second longest coastline in the world, with a length of more than 81,000 km total. Indonesia consists of 17,508 islands, the five largest of which are Papua, Kalimantan, Sumatra, Sulawesi, and Java. Java is the most populous island in Indonesia and in the world, with a population of 145 million in 2015 (57% of all Indonesia: BPS Indonesia, 2017). In fact, most of the population of Java Island lives in coastal megacities such as Jakarta, Surabaya, and Semarang (Firman, 2007). Meanwhile, coastlines are especially dynamic areas under strong environmental pressures, including coastal environmental degradation (Marfai, 2011). One of the coastal megacities with environmental problems in the coastal region is Semarang on Java Island. In the coastal region, Semarang is vulnerable to land subsidence (Marfai & King, 2007; Abidin et al., 2013; Lubis et al., 2011), sea level rise (Marfai & King, 2008), coastal flooding (Harwitasari & Van Ast, 2011), salt intrusion (Rahmawati et al., 2013), shoreline change (Dewi et al., 2016), and land use change (Handayani & Rudiarto, 2014). All of these problems are a major threat to community and coastal development.

Semarang is a flat, coastal urban area with a high level of industrial development and infrastructure (Marfai et al., 2008) that is vulnerable to land subsidence and sea level rise. As stated by Chaussard et al. (2013), many cities in Indonesia experience rapid land subsidence, including Jakarta, Surabaya and Semarang. Although Semarang is one of the big city in Indonesia, the number of population in Semarang is lower than in Jakarta and Surabaya according to census data in 2010 by Central Agency on Statistics data, and the subsidence rate is slower than Jakarta. However, this study measured the physical factor of coastal vulnerability; the social element was snubbed. Thus, this study selected Semarang as the study area instead of Jakarta or others city.

In Semarang, the land subsidence rate in the coastal region was found to be relatively fast, approximately 7 to 11 cm/year, and is caused mainly by alluvial deposits and groundwater extraction (Abidin et al., 2013). Land subsidence is the primary factor that causes coastal environmental degradation in Semarang. Coastal flooding in Semarang is worsened by land subsidence and sea level rise (Marfai & King, 2008). Sea level rise occurs because of climate change; land subsidence will expand into the inundated area and continuously increase the level of inundation (Harwitasari & Van Ast, 2011). Rahmawati et al. (2013) also stated that land subsidence and sea level change in coastal areas affects the fresh-saline water interface as a result of seawater movement toward land. According to Marfai et al. (2008), the shoreline dynamics in the Semarang coastal area are dominated by a sedimentation process, where the land subsidence is one of contributing factors that causes shoreline change (Dewi et al., 2016). Moreover, land use changes in Semarang are caused mostly by urbanization (Handayani & Rudiarto, 2014; Hadi et al., 2016) but have a significant impact on land subsidence (Gaffara et al., 2017). Therefore, the assessment of coastal vulnerability to enhanced land subsidence is a key issue at the national and international scales, especially for the coastal mega-city of Semarang.

Vulnerability is an essential concept in human-environmental research, but in general terms, vulnerability is the potential for loss (Wu et al., 2002; Cutter, 1996). Knowledge of vulnerability enables coastal scientists and policy-makers to anticipate the impact that could emerge because of a natural disaster in a coastal region (Klein & Nicholls, 1999). One of the most commonly used and simple methods for assessing the levels of susceptibility to hazards and risk within the coastal zone is the coastal vulnerability index (CVI: Gornitz, 1990; Gornitz et al., 1991, 1994; Ramieri et al., 2011). The CVI allows variables to be rated in a quantifiable manner to express the relative vulnerability of the coast due to physical changes caused by sea level rise (SLR), climate change, and anthropogenic impact, e.g., land subsidence (Denner et al., 2015; Addo, 2013). The CVI process is designed as a quick method for assessing coastal vulnerability; consequently, the list of parameters used is kept short, focusing on only the most important and easily assessed (Palmer et al., 2011). Moreover, Thieler and Hammar-Klose (1999) modified the CVI by reducing the number of variables in the Gornitz et al. (1994) index to be more effective and applicable. Palmer et al. (2011) and Bagdanavičiūté et al., (2015) introduced additional weightings focused on the specific requirements of estuarine locations and micro-tidal, low-lying areas, respectively. Addo (2013) also changed the vertical movement (relative sea level change) parameter in the CVI calculation, based on the variables in Gornitz et al. (1991), to include a local subsidence trend, which is assumed to be the same. According to Wöppelmann, et al. (2013), the vertical land movement is the same as land subsidence.

Remote sensing data can provide useful information about the landscape, including urban areas, coasts, and the ocean (Klemas, 2010; As-syakur et al., 2010; Tyo et al., 2006). Most of the studies in coastal areas are related to CVI and can use remote sensing data (e.g., Rao et al., 2008; Farhan & Lim, 2012; Li et al., 2016). Some of the CVI parameters usually obtained from remote sensing data include shoreline erosion, coastal slope, and relative sea level change. Vertical movement or land subsidence is very rarely used in CVI calculations because it is difficult to obtain (Martins et al., 2017); if anything, studies use ground station data (Addo, 2013; Cooper & Beevers, 2008). Therefore, it is an excellent opportunity to use land subsidence from remote sensing data as one of the parameters in the calculation of CVI. Land subsidence can be obtained from Synthetic Aperture Radar (SAR) of remote sensing data, where the Advanced Land Observing Satellite (ALOS) Phased Array type L-band SAR (PALSAR) is one of the most common sensors for calculating land subsidence (Sun et al., 2017; Bayuaji et al., 2010; Chaussard et al., 2013). Interferometric synthetic aperture radar (InSAR) is a recent technology used for land subsidence monitoring studies (Qu et al., 2014; Ferretti et al., 2015).

Index-based tools are particularly useful to make the first assessment of the vulnerability to SLR, land subsidence and coastal erosion impacts. The expression of the quantitative indices in the context of vulnerability is an essential step toward risk assessment and management. These methods would provide a relative quantification of coastal vulnerability to the effects and impacts of climate change and human activities. In this work, four sets of satellite data were utilized to identify the coastal area most vulnerable to land subsidence in the coastal mega-city of Semarang. This study was supposed to provide maps and data for supporting adaptation planning and regional Integrated Coastal Zone Management (ICZM) strategies. This study can be used as a rapid assessment and visualization of the relative vulnerability enhanced by land subsidence.

2. Study area

The research area is located in the coastal zone of the city of Semarang, Central Java, Indonesia. The coordinates are 60°55′5″S – 60°58′45″S and 110°17′18″E – 110°29′25″E. Semarang is in the eastern part of Central Java, which is directly adjacent to the northern coast of Java, as shown in Fig. 1. The total area of Semarang is 373.7 km^2 (Semarang, 2014).

Semarang's landscape consists of two major categories. The first type is a low-lying coastal area to the north, with relatively flat topography and a slope of approximately 0–2°. The second type is a mountainous area with a gradient up to 45° and altitude of approximately 350 m above sea level. The land use of the northern parts of Semarang is primarily residential and industrial areas, with a higher population density compared to the southern parts. Geologically, Semarang is on volcanic rock, sedimentary rock and alluvial deposits (Abidin et al., 2013).

3. Material and methods

3.1. Data sources

The first step for calculating the CVI addresses identification of the primary variables influencing the coastal vulnerability and coastal evolution in general. The identified parameters are listed in Table 1. Most of these parameters are dynamic and generated from different sources. The
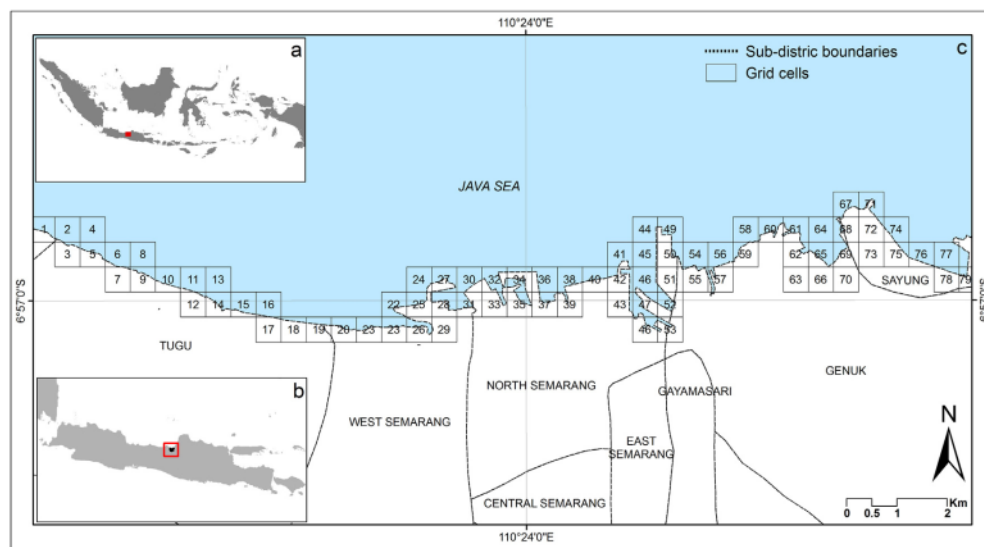

Fig. 1. Location of study area.

Table 1
Sources and period of the different usage parameters in the compiling of the CVI.

Parameters	Sources of data	Resolution	Period
Land subsidence	ALOS PALSAR imageries by Interferometric Synthetic Aperture Radar	10 m	2009–2010
Rate of shoreline change	Landsat 5 TM imagery was accessed at http://earthexplorer.usgs.gov/	30 m	1999 & 2009
Coastal slope	Diponegoro University conducted topography field survey	–	2007
Geomorphology	Land use data and IKONOS imagery from Diponegoro University	1 m	2008
Significant wave height	European Center for Medium-Range Weather Forecasts (ECMWF) was accessed at http://ecmwf.int/	1.5°	1994–2009
Mean tidal range	Field data was accessed from Indonesia Agency for Meteorology, Climatology, and Geophysics (BMKG)	–	2009
Sea level change	Altimeter satellite TOPEX/Poseidon was accessed at https://www.aviso.altimetry.fr/index.php?id=1599	0.5°	1993–2009
GPS data	Benchmark by field survey for verification		2009–2010

range of vulnerability for each parameter was divided into five categories, i.e., very low, low, moderate, high and very high (Gornitz et al., 1991; Pendleton et al., 2010). To develop a database for the coastal vulnerability assessment, we used land subsidence data, coastal slope data, shoreline change analysis, geomorphology data, mean tidal range data, mean significant wave height data, and SLR as parameters. Each parameter was measured in a grid cell known as the shoreline grid to measure the vulnerability for each parameter. This was used as the mapping unit and had a size of 500 m * 500 m. Thus, 79 shoreline grids were created. We assumed that this size was adequate for a uniform scaling of the data. Thus, some data were either upscaled or downscaled.

Since land subsidence is the major issue in Semarang, Indonesia, due to its location on young alluvial soil and its high social activity (Abidin et al., 2013), the CVI was calculated twice using six and seven parameters, with and without a land subsidence parameter, to elucidate the impact of land subsidence on the coastal vulnerability.

3.2. Coastal vulnerability index

The CVI was computed by Gornitz et al. (1991), Thieler and Hammer-Klose (1999), Doukakis (2005), and Diez et al. (2007) as the square root of the product of ordering risk (1 to 5 for each parameter) and divided by the total number of parameters. The parameters were ranked and are shown in Table 2. Each parameter was assigned a relative vulnerability value from 1 to 5, where 1 indicates very low vulnerability and 5 indicates very high vulnerability.

Unweighted and weighted parameters can be applied to the CVI; there are several previous studies that applied the unweighted parameters (Gornitz et al., 1991; Thieler and Hammer-Klose, 1999; Pendleton et al., 2005; Gaki-Papanastassiou et al., 2010; Di Paola et al., 2011; Addo, 2013; Kunte et al. 2014) and the weighted parameters (Doukakis, 2005; Diez et al., 2007; Rao et al., 2008; Duriyapong and Nakhapakorn, 2011; Yin et al., 2012). There is no convention in the literature for the weight assigned to the difference parameter comprising a CVI

(Kunte et al., 2014); however, equal weight of the CVI is used widely. The weighted CVI requires expert judgment to decide the rank each parameter (Duriyapong & Nakhapakorn, 2011). Furthermore, the weighted CVI is also influenced by personal judgment.

The CVI is calculated as the square root of the ranked variable and is divided by the total number of variables. The highest and lowest values of the CVI were determined to be in the range from 0.38 to 105.64, as in the following Eqs. (1) and (2) (Pendleton et al., 2010).

$$CVI_{6\ parameters} = \sqrt{\frac{SC*CS*G*MT*SL*SWH}{6}} \qquad (1)$$

$$CVI_{7\ parameters} = \sqrt{\frac{LS*SC*CS*G*MT*SL*SWH}{7}} \qquad (2)$$

where LS = land subsidence rate (mm/year), SC = shoreline change (m/year), CS = coastal slope (%), G = geomorphology, MT = mean tidal range (m), SL = relative sea level rise rate (mm/year), and SW = mean significant wave height (m).

The range value of CVI can be split into four equal parts (Gornitz et al., 1991; Diez et al. 2007), as quartiles (Pendleton et al., 2005; Abuodha and Woodroffe, 2006) or percentiles (Doukakis 2005). In this study, the CVI was divided into four risk levels by quantile classification. It classifies the quarters of an equal-sized group of CVI range values. The lowest range of CVI values designates low risk, followed by moderate risk, high risk and finally the highest range of values denoting a very high risk level of coastal vulnerability.

3.3. Physical parameters

3.3.1. Land subsidence (LS)

The synthetic aperture radar (SAR) satellite is an active remote sensing system that transmits microwaves in a side-looking direction and receives the signal reflected by the Earth's surface. The SAR image can focus on a point reflector on the ground by consistently summing thousands of sequential signals, thus generating a synthetic aperture

Table 2
Range for vulnerability ranking for CVI.

Parameters (Score value) (Pendleton et al., 2010)	Very Low (1)	Low (2)	Moderate (3)	High (4)	Very High (5)
Shoreline erosion (meters per year) (Pendleton et al., 2010)	>2.0	1.0–2.0	−1.0 to 1.0	−2.0–(−1.0)	<−2.0
Coastal slope (%) (Pendleton et al., 2010)	>1.420	1.20–0.90	0.90–0.60	0.60–0.30	<0.30
Geomorphology (Pendleton et al., 2010)	Rocky cliffed coast, fjords	Medium cliffs, indented coasts	Low cliffs, glacial drift, alluvial plains	Cobble beaches, estuary, lagoon	Barrier beaches, sand beaches, salt marsh, mud flats, deltas, mangrove, coral reefs
Mean significant wave height (meters) (Pendleton et al., 2010)	<0.55	0.55–0.85	0.85–1.05	1.05–1.25	>1.25
Mean tidal range (m) (Pendleton et al., 2010)	<0.99	1.0–1.99	2.0–3.99	4.0–6.0	>0.6
Relative sea level change (millimeters per year) (Pendleton et al., 2010)	<1.8	1.8–2.5	2.5–3.0	3.0–3.4	>3.4
Local subsidence trend (mm/year) (Gornitz and White, 1992)	<−1.0 Land rising	−1.0 to 1.0	1.0–2.0	2.1–4.0	>4.0 Land sinking

by manipulating the synthetic aperture method. By summing the complex numbers along a certain range, the proper focus can be achieved. The focus image contains both amplitude (backscatter) and phase (range) information for each pixel (Sandwell et al., 2011). The range resolution of an SAR image depends on the bandwidth and incident angle (Sandwell et al., 2011). Radar bandwidth is the chirp frequency defined by the satellite system as a sampling frequency to determine the range resolution of an SAR image. The incident angle is an angle between the ground surface normal line (vertical line) and side-looking line of the SAR satellite (Sandwell et al., 2011). The relationship between the range resolution, incident angle, and ground resolution are expressed as follows in Eq. (3) (Sandwell et al., 2011).

$$Ground\ resolution = \frac{Range\ resolution}{\sin\ incidence\ angle} \quad (3)$$

The interferometric synthetic aperture radar (InSAR) technique is a recently developed technology for land subsidence monitoring studies. The InSAR technique requires at least two SAR images. Those SAR images are taken by SAR satellite in the same area at a slightly different time and satellite position. The SAR image in the first observation is called the master image, and the second observation is the slave image. The InSAR technique utilizes the phase information of master and slave images and constructs the interferogram by taking the phase difference of those SAR images. The total phase difference or interferometric phase (ϕ_{intf}) between the corresponding complex pixel can be expressed as follows in Eq. (4) (Rocca et al., 2000):

$$\phi_{intf} = \phi_{flat} + \phi_{topo} + \phi_{defo} + \phi_{atm} + \phi_{noise} \quad (4)$$

where ϕ_{intf} is the interferometric phase, ϕ_{flat} is the flat Earth phase, ϕ_{topo} is the topographic phase, ϕ_{defo} is the phase due to surface displacement or subsidence, ϕ_{atm} is the atmospheric delay phase, and ϕ_{noise} is the measurement

noise. The flat Earth phase ϕ_{flat} can be removed through the interferogram flattening process (Ferretti et al., 2015). The phase due to noise ϕ_{noise} can be reduced by the adaptive filtering method (Goldstein and Wenner, 1998). If the phase of atmospheric delay ϕ_{atm} can be ignored, the remaining phase, ϕ_{intf}, can be represented by Eq. (5) (Rocca et al., 2000):

$$\phi_{intf} = \phi_{topo} + \phi_{defo} \quad (5)$$

The topographic phase ϕ_{topo} can be removed using a digital elevation model (DEM), and this process is called Differential Interferometric Synthetic Aperture Radar (DInSAR). After removing the topographic phase, the interferometric phase is equal to the following in Eq. (6):

$$\phi_{intf} = \phi_{defo} \quad (6)$$

where the phase due to surface deformation ϕ_{defo} is proportional to the travel path difference of the master image and slave image 2Δro, expressed as Eq. (7) (Rocca et al., 2000).

$$\phi_{defo} = 4\pi/\lambda\Delta ro \quad (7)$$

where λ is a wavelength of the SAR signal and 2 Δro is the travel path difference of the master image and slave image (2 indicates the round trip of the signal, from satellite to the target and back from the target to the satellite). The phase due to surface deformation ϕ_{defo} represents the Earth's surface movements relative to the satellite position. Subsidence means the Earth's surface moves away from the satellite position and uplift means the Earth's surface moves to the satellite position.

In this research, the SAR image was used from the PALSAR sensor, which was mounted on the ALOS, commonly abbreviated as ALOS PALSAR. The wavelength (λ) of ALOS PALSAR is 23.62 cm, and the bandwidth is 28 MHz (in fine single polarization mode). The 28 MHz bandwidth results in a range resolution of approximately 7 m. The incident angle of ALOS PALSAR is approximately

34.3° (EORC, 2008). From Eq. (3), using a 7-m range resolution and 34.3° incident angle results in an approximately 14-m ground resolution.

The land subsidence in Semarang from DInSAR was produced by the SAR images taken on December 14, 2009 (master image), and December 17, 2010 (slave image). The digital elevation model (DEM) from the Shuttle Radar Topography Mission (SRTM) was used for removing the topographic phase. An open-source SAR image processor, GMTSAR, was used for SAR image processing (Sandwell et al., 2014).

3.3.2. Shoreline change (SC)

A shoreline grid was created to be the measuring unit for the index calculation. However, it was applied to all parameters for measurement of the vulnerability. Each grid cell was categorized into one of five classes. The analysis of the shoreline change rate was conducted through the steps described below.

3.3.2.1. Coastal delineations.
A combination technique of the single band threshold of band-4 (TM B4) and false color composite (FCC) were used to delineate the coastline features. While the single band of both the 1999 and 2009 datasets was used for digitally slicing into the land and water features, we found that the FCC of the RGB 542 and other composites were used to visually obtain 20 values of the digital number (DN) threshold of water and land boundary, which was used for slicing. The result was a binary raster for water-land classes of 1999 and 2009, respectively. Each binary raster was converted into coastline vectors of the 1999 and 2009 feature sets. The result was polygon and polyline feature sets of the water-land class for the 1991 and 2009 feature sets.

3.3.2.2. Accretion and erosion extraction.
In the current study, there were only two coastline sets extracted, for 1999 and 2009; then, the combination of endpoint rate (EPR) and single transect methods were used to analyze coastline change. While the polygon feature from the previous step was used to indicate the accretion and erosion area trough overlay, the polyline set was used to determine if the point intersection of the transect casting locations changed (movement location). Thieler and Hammer-Klose (1999) explained that EPR was one of the simplest methods of the contemporary rate-of-change calculation methods, which uses only two shoreline positions. The rate was calculated by dividing the distance of the shoreline movement by the time elapsed between the earliest and latest measurements (i.e., the oldest and the most recent shoreline).

Baseline and single transects for measuring shoreline position movement were created using DSAS V 4.3 (Digital Shoreline Analysis System). Transect intervals used between the intersections of vertices were 50 m. The negative values were added to the shape length of the erosion transects, while the positive values were added for accretion. Marking for both signs was applied to all transects,

in which the accretion and erosion areas that were generated from the overlaid polygon of features was checked. The clip tool was used for distinctive transects in each shoreline grid. The next step in the change rate analysis was prepared by exporting the attribute table (database file) of the transect polylines, including the values of min, max, average, variant, and standard deviation.

3.3.2.3. Rate of accretion and erosion.
Calculating the rates-of-change of the coastline within each grid was employed using the statistics of the summary report from the previous step, formulated as follows in Eq. (8) (Kasim and Siregar, 2012):

$$Vc = \left(\frac{\mathrm{Lae}}{\sum \mathrm{Nae}} \right) . Y^{-1} \tag{8}$$

where Vc is the average of the rate-of-change of forward/backward moving shoreline in each shoreline grid (m y^{-1}), Lae and $\sum Nae$, respectively, were the overall shape length of transect polylines (m) and the number of transects within shoreline grids from data base report, and Y is the time elapsed for the coastline features analyzed (in the present study, this was 12 years, from 1999 to 2009).

3.3.3. Coastal slope (CS)

The coastal slope is the main aspect to be measured along with the coastal morphology in approximating the coastal vulnerability (Roa et al., 2008). On a low coast or flat coast, the impact of coastal inundation is higher and expanded inland. The coastal slope is a vulnerability signal to inundation and the possible rapidity of shoreline recoil, because low-sloping coastal regions should recoil faster than steeper regions (Pendleton et al., 2010).

The topography data from the field survey by Diponegoro University was interpolated to a digital elevation model (DEM). Considering the classes of the coastal slope based on Table 2, it was divided into five ranks to keep in view the condition that the lower of coastal slope value, the higher the vulnerability of the coastal area. The average percentage of the coastal slope was 0.01–0.33% for each of the shoreline grid cells. The vulnerability level ranges were high to very high.

3.3.4. Geomorphology (G)

The geomorphology is one of the coastal vulnerability variables that has a significant role in examining the coastal vulnerability, due to the correlation with land use along the coast. Some studies have shown geomorphology responses to the coastal vulnerability, e.g., Chadha et al. (2005), Banerjee (2005), Rao et al. (2008), Mahapatra et al. (2015). Landform and composed material prefer a certain level of tolerance to erosion (Thieler and Hammer-Klose, 1999). Rocky cliffed coasts and fjords offer high resistance to erosion. However, barrier beaches, sand beaches, salt marsh, and mud offer low resistance.

The geomorphology mapping was derived from the land use data, and land cover data, since the geomorphology has

an important role for the land surface. Hence, the association of land use, land cover and geomorphology were used for the visual interpretation of IKONOS imagery, and integrated with the coastal map from the Indonesian Coastal Environment Agency and Geology map.

3.3.5. Significant wave height (SWH)

SWH is the mean trough to crest in meters of the highest one-third of all the wave heights during a 20-min measuring time (NBDC and NOAA, 2017). It is utilized as a replacement for wave energy and is considered an important parameter in assessing coastal vulnerability. SWH energy transports the coastal sediment, thereby influencing coastal erosion and the coastal accession process (Gaki-Papanastassiou et al., 2010). Wave energy is directly associated with the square of the wave height following Eq. (9):

$$E = \frac{1}{8} pgH^2 \tag{9}$$

where E denotes the energy, H express SWH, p indicates water density and g designate the acceleration due to gravity. The wave height square is a function of coastal transportation (Pendleton et al., 2005; Thieler and Hammar-Klose, 2000). Increasing the wave energy leads to an increase of wave height, which causes attrition inland by the erosion process and inundation of another side. Hence, low wave height was considered to correspond to low coastal vulnerability, and vice versa.

This study used extracted satellite image data from 1994 to 2012 with observational data at 6-hour intervals in the domain of the Java Sea and the surrounding areas. The spatial resolution of the significant wave height was 1.5°. In situ observation of wave data was rare. Hence, satellite altimetry was the primary data for extracting the significant wave high. These seasonal climate effects to wave height were not considered in this study. Significant wave height data were interpolated to obtain the spatial distribution of the shoreline grid cells and followed Table 2 to classify the level of vulnerability.

3.3.6. Mean tidal range (MT)

Tidal range is the term describing the vertical change between the maximum high tide and the minimum low tide and is related to tidal flooding (Diez et al., 2007; Doukakis, 2005). The tidal range influences both permanent and episodic tidal flooding (Pendleton et al., 2010). A coastal area is judged to be highly vulnerable if it experiences a high tidal range, whereas the large tidal range is connected to strong tidal currents that impact coastal behavior (Gornitz et al., 1991; Rao et al. 2008; Mahapatra et al., 2015). Some previous studies have assigned the mean tidal range as a parameter for coastal vulnerability (Gornitz et al., 1994; Doukakis, 2005; Diez et al., 2007; Di Paola et al., 2011; Duriyapong and Nakhapakorn, 2011; Yin et al., 2012 Addo, 2013).

Tidal data were obtained from the Indonesian Agency for Meteorology, Climatology, and Geophysics (BMKG)

of Semarang. Hourly data from January-December 2009 from 2 stations along the coast in Semarang, Indonesia, were averaged to produce the mean tidal range. Following Table 2, it was classified into five ranks.

3.3.7. Sea level rise (SLR)

The SLR influences the change in tides. Therefore, it is an important parameter in studying coastal vulnerability. Over 70% of global coastlines were projected to experience sea level change of up to 20% (Church et al., 2013). In this study, a high rate of SLR was designated to correspond to high coastal vulnerability and vice versa. The classification of SLR followed Table 2.

The change in SLR was obtained from satellite altimeter TOPEX/Poseidon over a period of 17 years (from October 1992 to July 2009). The format of the data was NetCDF (Network Common Data Form) with a grid system of 0.250×0.250 (27.8 km × 27.8 km). Global mean sea level (GMSL) was calculated after eliminating annual and semi-annual signals including screening seasonal patterns, atmospheric pressure, barometer process, and the influence of wind. The SLR was extracted by applying ODV (Ocean Data View) software in text format (*.txt) and followed by data processing, e.g., masking of the study area, then sorting and filtering. The data were interpolated and extracted from raster to feature point.

4. Results and discussion

This study is a continuation of previous research (http://www.pps.unud.ac.id/thesis/pdf_thesis/unud-1279-1113081654-jurnal_husnayaen.pdf). We calculated the seven parameters of CVI as well as this current study. However, this current study utilized the land subsidence data from the latest technology to measure the displacement by DInSAR method, while the previous study from interpolation data of the field survey. Hence, this study enhanced the unit data from centimeter to millimeter. This current study provided more detail information and high accuracy.

4.1. Six parameters of CVI (shoreline, slope, geomorphology, SWH, tidal range and SLR)

Shoreline, slope, geomorphology, SWH, tidal range and SLR are the commonly used parameters for CVI (Kumar et al., 2010; Kumar and Kunte, 2012). Fig. 2 represents these parameters. The results were generated from data in Table 1 and classified according to the classification rule in Table 2. The coastal slope (Fig. 2b) and SLR (Fig. 2f) in the area were classified as very high risk of coastal vulnerability. However, significant wave height and mean tidal range were classified as low vulnerability. Shoreline and geomorphology classification varied from very low to very high.

The shoreline is shown in Fig. 2a. A shoreline is a viable ecology that advances under both environmental and social influences. The sensitivity of the coast can be measured by
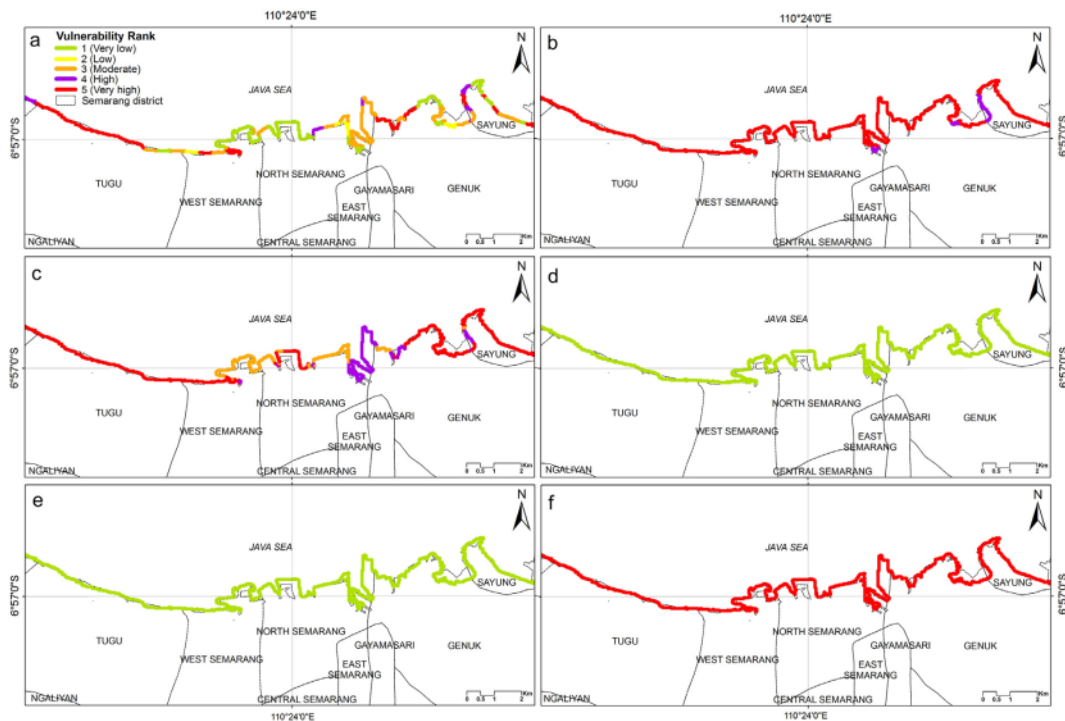
Fig. 2. Vulnerability rank of (a) shoreline, (b) coastal slope (c) geomorphology, (d) significant wave height, (e) mean tidal range, and (f) sea level rise.

coastal change. Erosion and accretion (accumulation of sediment) are natural events experienced by the shoreline by means of donating and receiving activities. This association is of certain importance due to its influence on social needs and growth of the shore. Furthermore, the erosion is believed to be a risk not only because of physical development but also by extending the usages of the beach through economic and tourism activities (Domínguez et al., 2005). In line with this study result, the shoreline change in Semarang is caused by social and economic activity, as well as land use change (Hadi et al., 2016). However, it is also influenced by physical processes, e.g., significant wave height, high tides and sea level rise. In addition to these causes, Marfai (2011), mention that wind has contributed to the erosion along the Semarang coast. Hence, Semarang is impacted by coastal inundation, erosion, and accretion (Bird & Ongkosongo, 1980; Marfai et al., 2008). Due to the shoreline change, there have been some losses to public facilities such as roads, tourism areas, aquaculture, and coastal settlements. From this study, most of the shoreline change has occurred in Tugu and some areas in the Genuk sub-district.

The coastal slope in Semarang was categorized as having very high risk of coastal vulnerability, as shown in Fig. 2b. The slope value was < 0.30%, which means a flat area. According to this result, the coastal area in Semarang has a low relief and is composed of alluvium, marsh and sand beaches. Considering the results of the interpretation of land use and land cover, the Semarang coast was categorized by geomorphology and vulnerability level according to Table 2. The geomorphology of each shoreline grid cell in Semarang, Indonesia, has areas of moderate, high and very high risk, as shown in Fig. 2c.

The mean value of the significant wave height was 0.28–0.32 m for each shoreline grid cell. Meilistya et al. (2012) studied the significant wave height through field measurements in Semarang, and the results were 0.58 m (Meilistya et al., 2012), while the significant wave height from the conversion results of wind data (2001–2010) was 0.71 m. This study result was similar to the value of the significant wave height data from ECMWF in Fig. 2d. According to the calculation, the average of the tidal data was 0.85 m. Hence, the class of the mean tidal range data was very low in terms of the coastal vulnerability, as shown in Fig. 2e. However, the range value of SLR was 5.87–5.90 mm/year for each shoreline. The vulnerability class was very high vulnerability for all shoreline grid cells, as displayed in Fig. 3f.

These six parameters show that the level of coastal vulnerability in Semarang, Indonesia, is influenced by shoreline change and geomorphology because these values vary from very low to very high. However, other parameters only have one class, which means that they will have the same value at all sites along the coast. Hence, when
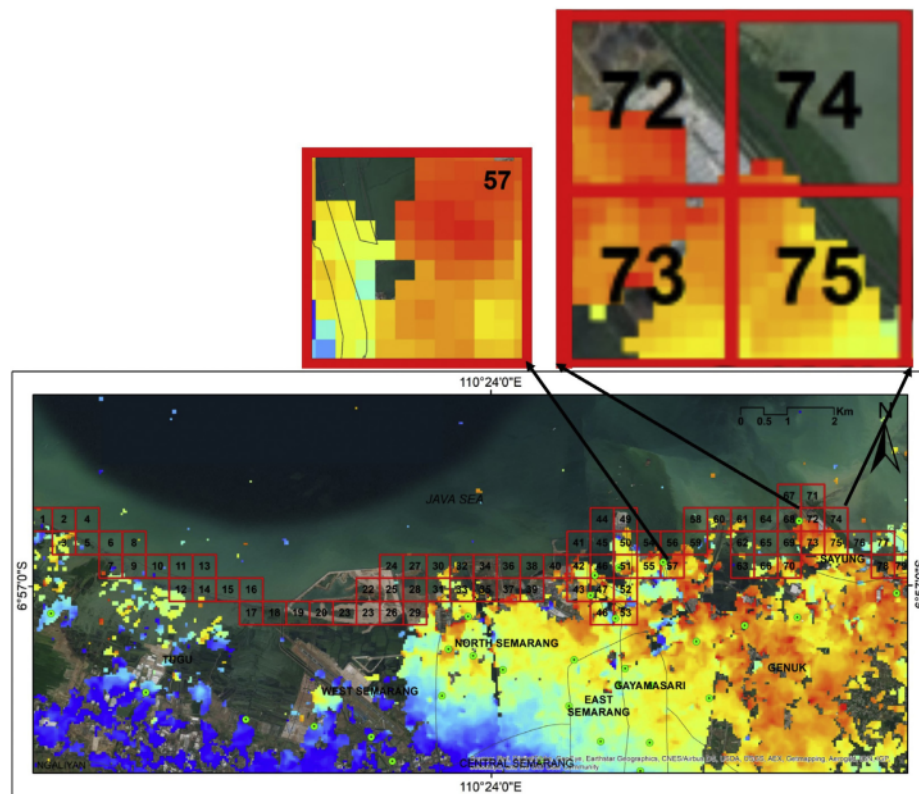
Fig. 3. Land subsidence distribution in Semarang and some examples of grid cells with high subsidence.

the CVI calculation is applied, the result will be constant with no variation.

4.2. Land subsidence

The DInSAR for land subsidence in Semarang is produced by two SAR images, namely, the SAR images that were taken on December 14, 2009 (master image), and December 17, 2010 (slave image). The time difference of those SAR images is 368 days (almost one year). The subsidence resulting from the DInSAR was validated using the subsidence results from GPS. GPS data were obtained from the geodetic survey. A total of 35 GPS points were utilized in this research to verify the land subsidence in Semarang. One point is used as the reference point, and 34 points are used as measurement points. We assumed that the reference point is constant; there is no subsidence event at this reference point. We used the same GPS reference point for the DInSAR results. The measurement points are relative to the reference point. The land subsidence variable has a value range from 0 to 9.9 cm/year for each shoreline (see Fig. 3).

These values were categorized as low to very high vulnerability. The cause of subsidence in Semarang is the consolidation of clay within the aquifer systems due to the extensive groundwater withdrawal, especially in the lowland area (Marfai & King, 2007). The lithology of this area is alluvial, composed of soft clay soil deposits. It is important to notice that such subsidence is permanent, as stressing and changing the pressure within the aquifer system affects it, causing the groundwater supply to decrease. Even though the groundwater level can eventually be recharged, the land surface will not return to its original position (Marfai & King, 2008).

A spatial analysis shows that the impact of land subsidence along the Semarang coast is most apparent in northern Semarang, the Sayung sub-district, and the Genuk sub-district. The spatial map of land subsidence is shown in Fig. 3. Some grid cells have a large value, for example, grid cell numbers 57, 72, 73, 74 and 75, and others (see Fig. 3, enlarged parts). According to Google Maps, these areas are port and industrial areas, in which some large companies utilize the huge volume of water to achieve target production. This condition certainly leads to the land subsidence in this area and thus influences the coastal vulnerability.

The level of vulnerability for land subsidence (Fig. 4) could be generated from Fig. 3. The value of land subsidence for the shoreline grid in Fig. 3 was classified according to Table 2. Fig. 4 shows the rank of land subsidence
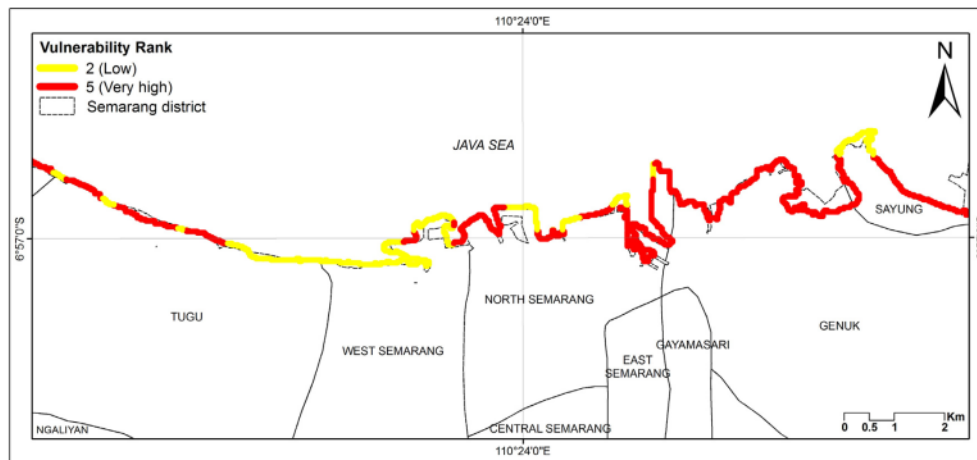
Fig. 4. Vulnerability rank of land subsidence in Semarang, Indonesia, to coastal vulnerability.

vulnerability. There were two classes, low (−1.0 to 1.0) and very high (>4.0 land sinking). The shoreline along the Genuk sub-district has been sinking and was categorized as very high vulnerability. For the most part, the shorelines in Sayung, northern Semarang and some areas in the Tugu sub-district were classified as very high vulnerability. The land use for these areas are settlement and industry. However, the western Semarang sub-district was categorized as low vulnerability. Furthermore, Figs. 2 and 4 were utilized for calculating the CVI 7 parameters.

4.3. Comparison between six and seven parameters of CVI

As is widely known, the land subsidence in Semarang occurs intensively due to the clay soil composed of young alluvium, which accumulated from the river (Abidin et al., 2013). Moreover, Semarang has been intensively developed; the young alluvium is overloaded by the building. Furthermore, the industrial area required the water use for production purposes. Hence, intensive groundwater withdrawal (Marfai & King, 2007) has occurred, especially in North Semarang, Genuk and Sayung. Due to the intensive land use in the coastal area, which affected the land subsidence, we assumed that land subsidence is one cause for coastal vulnerability in Semarang.

From this study, we could declare that land subsidence has a role in the coastal vulnerability of Semarang, Indonesia. The CVI of 6 parameters and seven parameters with and without the land subsidence parameter were compared. The seven parameters area of the CVI do not have the same coverage extent as the six parameters of CVI, as seen in Fig. 5.

Fig. 5a is six parameters of the CVI and Fig. 5b is seven parameters of the CVI. The area was divided into six parts to enhance the different CVI analyses. Fig. 6a shows the most vulnerable area is part 1a, however, for Fig. 5b is 1b, 5b and 6b. This is because the slope, SWH, tidal range

and SLR only have one class along the study area. Hence, the shoreline and geomorphology have more influence on the level of coastal vulnerability. The occurrence of shoreline change is intense in part 1a, and the geomorphology included a salt marsh, sand, and mangrove, which were categorized as very vulnerable according to Table 2; thus, part 1a is very vulnerable. However, as shown in Fig. 5b, the subsidence occurrence is intense in North Semarang, the Genuk and Sayung sub-districts, or parts 4b, 5b and 6b. Thus, this area is categorized as very high vulnerability according to Table 2. By applying the CVI, we found that the Tugu, Genuk and Sayung sub-districts have very high coastal vulnerability.

Generally, the coastal vulnerability as estimated by CVI significantly increases when the land subsidence parameter is included, for example, in parts 3b, 4b, 5b and 6b. However, parts 1b and 2b decreased when the land subsidence was added. This occurred because we used the high accuracy land subsidence data. According to the DInSAR analyses, the accuracy is within mm. However, the mapping unit for CVI is the shoreline grid, which covers an area of 500 m * 500 m. This means that in one shoreline grid cell, a large number of land subsidence pixels are calculated, which leads to a high accuracy of land subsidence. Thus, we could easily categorize the land subsidence; no movement of the land was categorized as low vulnerability, and land sinking of >4 mm was classified as high vulnerability. Hence, the area of land subsidence can be measured with high precision. The land subsidence in parts 1b and 2b occurred only in some of the shoreline grid. Thus, this influences the seven-parameter calculation of the CVI. When using the calculation with six parameters, parts 1a and 2a were only influenced by shoreline change and geomorphology, which were categorized as high to very high. However, when we added the land subsidence, because some areas do not experience land subsidence, parts 1b
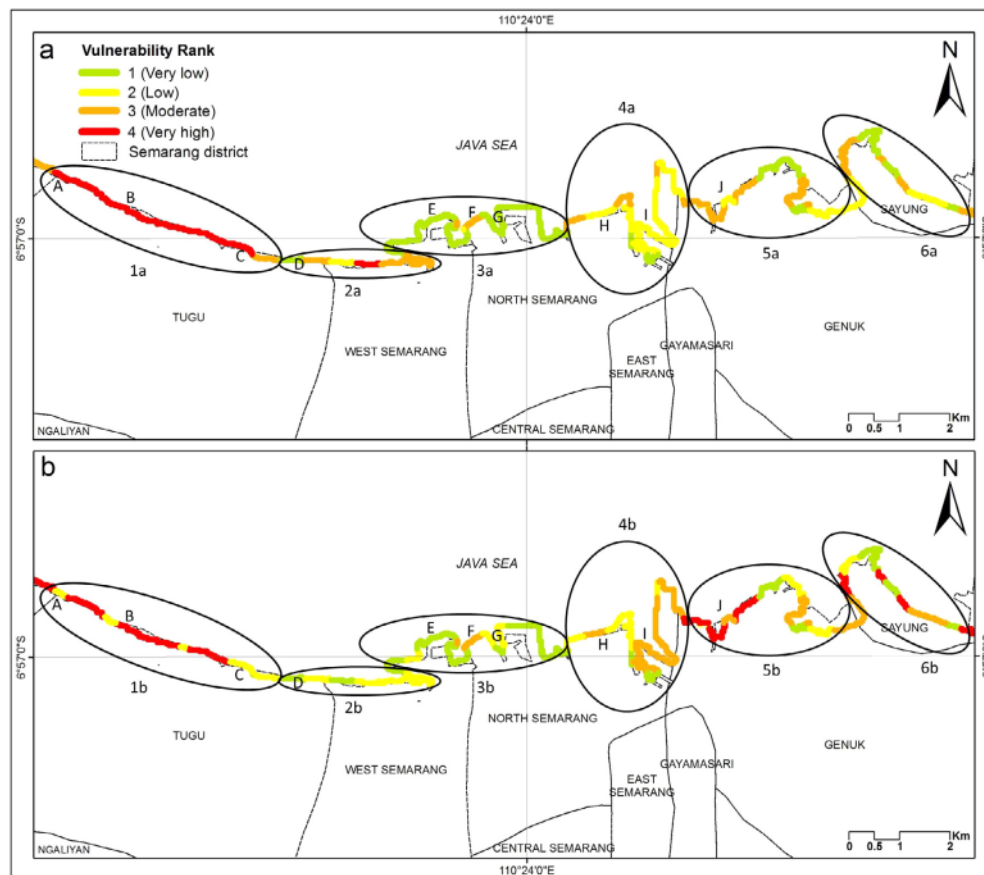
Fig. 5. Comparison of the CVI in Semarang, Indonesia (a) 6-parameters CVI (b) 7-parameters CVI.
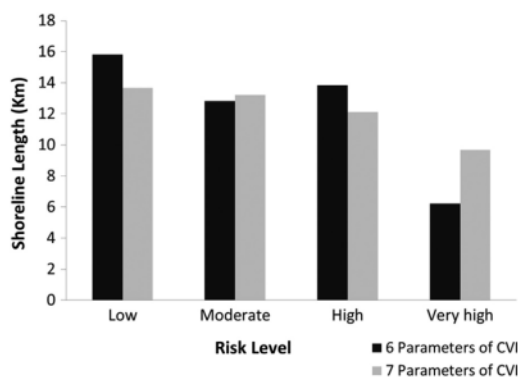

Fig. 6. Comparison of vulnerability determined by CVI using 6 and 7 parameters.

and 2b exhibited a decrease in the level of coastal vulnerability.

According to the CVI analysis in Table 3 and Fig. 6, the shoreline with low coastal vulnerability decreased by 4%, or 2.1 km, of the total length of the coastline, that is, from 15.8 km to 13.7 km. The coast with a very high risk level of coastal vulnerability increased by 7% when adding the land subsidence, and the total with very high vulnerability increased by 20%, to 48.7 km. Hence, the high risk of the coastal vulnerability increased by 3.4 km, from 6.2 km to 9.7 km. However, when applying seven rather than six parameters in the CVI, the amount of shoreline at a moderate risk level only changed by 1%, or 0.42 km. The comparison of the percentage risk vulnerability for the 6-parameter CVI shows that the proportion of coast at low risk is 32% and the proportion at very high risk is 13%; the proportions at moderate and high risk are 26% and 28%, respectively. However, based on the 7-parameters CVI, the percentage of the coastline at low, moderate, high and very high risk are 28%, 27%, 25% and 20%, respectively. The significance of the percentage for very high risk vulnerability increased by adding the land subsidence parameters.

The CVI is applicable to all areas, and the user can add parameters to describe the relevant problems. However, the classification of a range for the CVI is based on the lowest and highest values and is divided into four classes. This

Table 3
Percentage of CVI for each level of vulnerability.

Risk level	Length (km) 6 parameters	% (6 parameters)	Length (km) 7 parameters	% (7 parameters)
Low	15,815	32	13,680	28
Moderate	12,806	26	13,227	27
High	13,836	28	12,102	25
Very high	6220	13	9668	20
Total	48,677	100%	48,677	100%

means the range classes should be low to very high, even though the area analyzed is in good coastal condition. This condition may occur because the rank is defined only by the area itself, meaning that there is no range standard value for low, moderate, high or very high. To prevent this condition, we suggested a comparison with other studies or field survey data. The field survey was conducted during the end of December 2017 to early of January 2018, due to the rainy season difficult to access some places. Table 4 shows the validation image from Google Earth (GE) and field survey. The GE images show the different condition of visited area year by year, however, the field survey shows the current condition.

4.4. Ground check and validation

The field survey was conducted from the third week of December 2017 to the first week of January 2018. The ground check was conducted from west to east part along Semarang beach. However, some area in eastern part of Semarang were prohibited from accessing due to the private area of the companies for example in Sayung; and some areas were difficult to visit due to the muddy areas for instance in Genuk and Tugu sub-districts. Nevertheless, the representative locations were selected and visited for ground check and validation. The Fitzpatrick Lins Equation (1981) was applied to decide the number of samples.

$$N = \frac{Z^2 pq}{E^2} \tag{10}$$

N = Number of sample
Z = Level of confidence according to the standard normal distribution (for a level of confidence of 80%, z = 2; 95%, z = 1.96, for a level of confidence of 99%, z = 2.575)
p = Estimated proportion of the population that presents the characteristic (when unknown p = 50)
q = 100 − p
E = Allowable error

In this study, the number of population was unknown, to apply Eq. (10), we decided the level of confidence was 95% and allowable error 50% from p. Hence, 15 points were required to verify this study as pointed in Fig. 5 (A)–(J).
There were four categories of vulnerability level (i.e., Very low, Low, Moderate and Very high). To compare

whether 6 or 7 parameters of CVI is more suitable for CVI, we selected the location for the survey by identifying the change of CVI 6 to CVI 7. There were 16 cases of changing (e.g., Very low to Very low, Very low to Low, Very low to Moderate, Very low to Very high, Low to Very low, etc.). However, according to Fig. 5, there were only 11 cases of changing, 6 cases were unavailable (i.e., Very low to Moderate, Very low to Very high, Low to Very high, Moderate to Very low, Very high to Very low, and Very high to Moderate). Table 4 shows the condition of ground check by field survey and comparison of GE images year by year.

The CVI 7 parameters are more suitable for coastal vulnerability in Semarang. It means that the land subsidence has been influencing the coastal vulnerability in Semarang. For example in Table 4 ID A, C and G, by applying CVI 6 parameters showed Very high, High, and Low, respectively. Contrariwise, by utilizing CVI 7 showed the low condition as same as the field survey. CVI 6 parameters generated 53% of overall accuracy and 93% of overall accuracy for CVI 7. Hence, the by adding land subsidence parameter, the accuracy increased 40%.

Kappa coefficient (K_{hat}) is often used in remote sensing validation to measure the agreement between interpretation and real condition in the field as follow Eq. (11) (Lillesand & Kiefer 2000).

$$\widehat{K} = \frac{observed\ accuracy - change\ agreement}{1 - change\ agreement} \tag{11}$$

By following Eq. (11), we calculated the agreement between field survey and CVI (six and seven parameters). CVI six parameters indicated fair agreement (0.31). However, CVI 7 directed very good agreement (0.90)

The local government of Semarang has been aware about the coastal vulnerability. Thus, they are protecting the coastline by planting mangroves, managing the drainage, installing breakwater and wall along the beach. By comparing the GE image from Table 4, it shows the significantly changing of coastline (i.e., ID A, B, E, G and J) by the government mitigation and adaptation to the coastal vulnerability in Semarang. However, the government actions were insufficient to hold the continuation of the coastal vulnerability due to land subsidence for example in Table 4 (ID F, I and J). ID F shows the water as the same high with the wall; ID I (picture a) shows the water over the wall, and moreover, the survey in 2010 shows tidal flood around Tanjung Mas area; ID J (picture c and d)

show the fishermen village lower than the road and flooded.

4.5. Erosion and accretion

According to this study, erosion and accretion were calculated for each sub-district in a coastal area of Semarang, Indonesia, as seen in Fig. 7. This shows the statistical values of the accretion and erosion rates from Landsat 5 TM in 1999 and 2009. This analysis was accorded to the length of each transect and shoreline grids. The accretion in the Tugu sub-district was 0.04 km^2, and the erosion was 0.65 km^2. Due to the coastal erosion and seawater inundation in the Tugu sub-district, the land function decreased, and the direct impact of the shoreline change in this area is that marine aquaculture farmers lost revenue. The West Semarang sub-district is located in the river mouth area and has several man-made structures, e.g., dikes and floodway canal. This area was conquered by sedimentation material from the upper catchment area (Marfai and King, 2007). According to the shoreline extraction from Landsat 1999 and 2009, the West Semarang sub-district was the largest accretion area with approximately 0.58 km^2, and 0.04

km^2 of erosion. The North Semarang sub-district was built up by man-made infrastructure, e.g., reclamation, harbor, and supporting structures (Marfai and King, 2007). This area has been developed for economic purposes. The accretion in North Semarang was 0.49 km^2, and erosion was 0.26 km^2. The accretion in the Genuk and Sayung sub-districts was 0.17 km^2, and the erosion was 0.23 km^2.

Fig. 7 shows all the erosion and accretion along the coastal area in Semarang, Indonesia. The Tugu sub-district is dominated by erosion and West Semarang is dominated by accretion. During the western monsoonal season, the SWH increases extremely (Shanas and Kumar, 2014). Furthermore, the energy of the SWH transports the coastal sediments (Gaki-Papanastassiou et al., 2010) and the SWH indicates the movement of coastal sediments (Doukakis, 2005). Because erosion and accretion is the process of achieving a coastal balance, the coastal sediment from the Tugu sub-district moves to western Semarang. Moreover, the straight coastline and geomorphological conditions of the Tugu sub-district allow the sediment to be transported far away from Tugu to West Semarang. However, in the Genuk and Sayung sub-district of North Semarang, erosion and accretion occurred in the same location, particularly in

Table 4
Ground check by field survey and comparison of GE images year by year.

ID	Location	Google Earth	Google Erath	Field Survey
A	Around Mangkang Indah Beach (Tugu sub-district) (1 Location)	26 September 2002	30 April 2009	Field Survey: 29 December 2017 Mangroves covered in the first line and fishpond in the second line from the sea. CVI 6: Very high CVI 7: Low Real condition: Low

(Continued on next page)

Table 4 (*continued*)
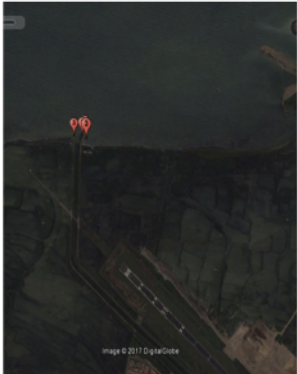
ID	Location	Google Earth	Google Erath	Field Survey
B	Around Mangunharjo Beach, (Tugu sub-district) (1 Location)	26 September 2002	28 May 2008 18 September 2017	Field Survey: 29 December 2017 In the east area of the survey point, the abrasion occurred. Thus, the local government planted mangroves along the river to protect the area. Figure 2002, 2008 and 2017 showed the conditions of the beach before and after mangrove planted. The picture was taken close to the river, due to the muddy area, the beach could not be accessed CVI 6: Very high CVI 7: Very high Real condition: Very high
C	North part of Marron Beach (Tugu sub-district) (1 Location)	22 Apri 2005	28 February 2016	Field Survey: 2 January 2018 In this area dominated by fishpond and mangroves CVI 6: High CVI 7: Low Real condition: Low

Table 4 (*continued*)

ID	Location	Google Earth	Google Erath	Field Survey
D	Maroon Beach Tourism Semarang (Tugu sub-district)(2 Locations)	6 August 2007	13 April 2012	Field Survey: 24 December 2017 No change in this area CVI 6: Low CVI 7: Low Real condition: Low
E	Marina Beach (West Semarang Sub-district)(1 Location)	31 May 2003	22 April 2010	Field Survey: 24 December 2017(Reclamation beach)CVI 6: Very lowCVI 7: Very lowReal condition: Very low

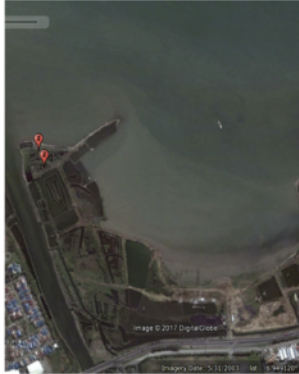(*Continued on next page*)

Table 4 (*continued*)
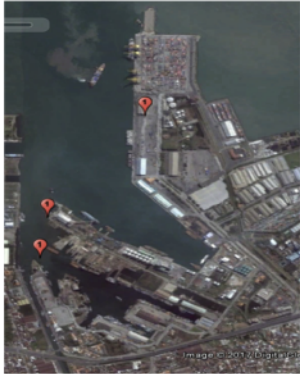
ID	Location	Google Earth	Google Erath	Field Survey
F	Marina Beach (West Semarang Sub-district)(1 Location)	31 May 2003	22 April 2010	Field Survey: 22 December 2017 Installed breakwater and wall along the beach CVI 6: Very high CVI 7: Very high Real condition: Very high
G	Baruna Beach (North Semarang Sub-district)(1 Location)	31 May 2003	18 September 2017	Field Survey: 22 December 2017 Installed breakwater (jetty) along the beach CVI 6: Very low CVI 7: Low Real condition: Low

Table 4 (*continued*)

ID	Location	Google Earth	Google Erath	Field Survey
H	Around Pantai Cipta (North Semarang Sub-district)(2 Locations)	31 May 2003	6 June 2010	Field Survey: 22 December 2017 Reclamation planed CVI 6: Very high CVI 7: Very high Real condition: Very high
I	Around Pelabuhan Tanjung Mas (North Semarang Sub-district)(2 Locations)	31 May 2003	27 June 2010	Field Survey: 19 December 2017 (a) Picture from Google map, this area is industry area and prohibit to enter. (b, c and d) Installed wall along the beach for prevent the tidal flood

Table 4 (*continued*)

| ID	Location	Google Earth	Google Erath	Field Survey
				 Field Survey: June2010 (Source: Mr. Helmi). Tidal flood inundation around Tanjung Mas port and Industry area in North Semarang. CVI 6: Low CVI 7: High Real condition a figure: Very high Real condition b, c, d figure: High
J	Around Tambak Lorok (North Semarang Sub-district)(3 Locations)	 31 May 2003	 18 September 2017In 2017, the local government of Semarang restored the city drainage by manage the east flood canal river, establish spun pile and tidal flood wall.	 Field Survey: 19 December 2017 (a) One of beach condition behind the spun line CVI 6: Very high CVI 7: Very high Real condition: Very high (b) Beach condition after installed tidal flood wall CVI 6: Low CVI 7: High Real condition: High (c, d) Subsidence impact to Fisherman villages in Semarang CVI 6: High CVI 7: Very High Real condition: Very high
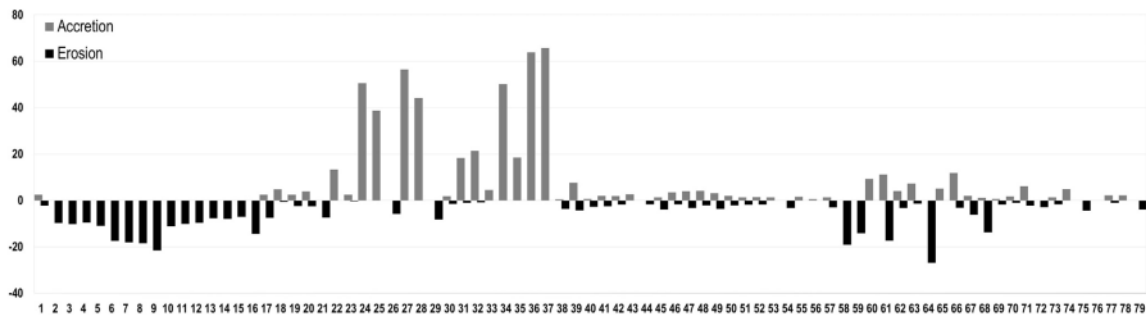
Fig. 7. Statistical values of accretion and erosion rates.

grids 38 – 79, due to the curve of the shoreline and a fairly large grid area; the energy for transporting the sediment is restrained in the cavity or basin coastline.

The average erosion of each transect was approximately 4.05–269.11 m. Approximately 52.13% or 0.03–65.71 m/year of accretion occurred along the Semarang coast; meanwhile, approximately 47.87% or 0.08–26.10 m/year of erosion occurred on every shoreline grid, showing how dynamic the coast is in Semarang. According to Marfai et al. (2008), Semarang is one of the most dynamic areas of sedimentation processes in Central Java. Regarding this shoreline change problem, the local government has been trying to mitigate this problem by constructing a wall and wave breakers along the coast. However, this problem still exists today.

5. Conclusion

Coastal vulnerability index assessments can provide insight into the relative potential of coastal changes due to land subsidence in Semarang, Indonesia. However, the vulnerability depends on the geomorphological conditions of the area, as the geomorphology is influenced by the level of shoreline change.

From this study, we could state that land subsidence influenced the coastal vulnerability in Semarang. By using the CVI calculation with six and seven parameters (i.e., without and with land subsidence parameters), we could measure that the high coastal vulnerability areas in Semarang increased by up to 7% by adding the land subsidence data. By overall accuracy, CVI 7 parameters showed 40% higher accuracy compared to CVI 6 parameters. Moreover, by Kappa coefficient, CVI 7 parameters indicated very good agreement (0.90) and CVI 6 parameters indicated fair agreement (0.31).

The high coastal vulnerability area occurred along 20% of the total length of the Semarang coast, i.e., 9.7 km of 48.7 km total. By using 7 parameters in the CVI, which added land subsidence as one parameter, we found that the length of coast in Semarang at low, moderate, high and very high vulnerability are quite equal, i.e., 28%, 27%, 25% and 20%, respectively. The increases in high vul-

nerability area due to land subsidence occur mostly in the Genuk and Sayung sub-districts and some parts of the North Semarang sub-district, because the land subsidence is increasing intensively in this area. This area is known as an industrial and settlement area.

The CVI method is quite simple and applicable to all areas. In this study, we were able to measure the level of risk of coastal areas in Semarang. Hence, we recommend that these results can be applied to Integrated Coastal Zone Management (ICZM) strategies.

However, this study stated that land subsidence has an essential role in coastal vulnerability, the advanced study is recommended to conduct since this study only considered the physical factor. Hence, the future study will continue to measure the social factor to coastal vulnerability.

References

Abidin, H.Z. et al., 2013. Land subsidence in coastal city of Semarang (Indonesia): characteristics, impacts and causes. Geomatics. Nat. Hazards Risk 4 (3), 226–240. https://doi.org/10.1080/19475705.2012.692336.

Addo, K.A., 2013. Assessing coastal vulnerability index to climate change: the case of Accra-Ghana. J. Coastal Res. 65 (SP2), 1892–1897. https://doi.org/10.2112/SI65-320.1.

Abuodha, P.A., Woodroffe, C.D., 2006. Assessing vulnerability of coasts to climate change: a review of approaches and their application to the Australian coast. Wollongong, A selection of Papers from Coast GIS 2006, Australian National Centre for Ocean Resources and Security University of Wollongong, Australia.

As-syakur, A.R., Osawa, T., Adnyana, I.W.S., 2010. Medium spatial resolution satellite imagery to estimate gross primary production in an urban area. Remote Sens. 2 (6), 1496–1507. https://doi.org/10.3390/rs2061496.

Bagdanavičiūtė, I., Kelpšaitė, L., Soomere, T., 2015. Multi-criteria evaluation approach to coastal vulnerability index development in micro-tidal low-lying areas. Ocean Coast. Manag. 104, 124–135. https://doi.org/10.1016/j.ocecoaman.2014.12.011.

Balica, S.F., Wright, N.G., van der Meulen, F., 2012. A flood vulnerability index for coastal cities and its use in assessing climate change impacts. Nat. Hazards 64 (1), 73–105. https://doi.org/10.1007/s11069-012-0234-l.

Banerjee, A., 2005. Tsunami deaths. Curr. Sci. 88 (9), 1358.

Bayuaji, L., Sumantyo, J.T.S., Kuze, H., 2010. ALOS PALSAR D-InSAR for land subsidence mapping in Jakarta, Indonesia. Can. J. Remote Sens. 36 (1), 1–8. https://doi.org/10.5589/m10-023.

Bird, E.C.F., Ongkosongo, O.S.R., 1980. Environmental Changes on the Coasts of Indonesia. United Nation University Press, Tokyo.

BPS (Central Agency on Statistics), <https://www.bps.go.id/QuickMap?id=0000000000> (accessed on 22 December 2017).

Chadha, R.K. et al., 2005. The tsunami of the great Sumatra earthquake of M 9.0 on 26 December 2004 – Impact on the east coast of India. Curr. Sci. 88 (8), 1297–1301.

Chaussard, E., Amelung, F., Abidin, H., Hong, S.H., 2013. Sinking cities in Indonesia: ALOS PALSAR detects rapid subsidence due to groundwater and gas extraction. Remote Sens. Environ. 128, 150–161. https://doi.org/10.1016/j.rse.2012.10.015.

Church, J. et al., 2013. Sea Level Change. In: Stocker, T. (Ed.), Climate Change 2013 The Physical Science Basis. Contribution of Working Group I to the Fifth Assessment Report of the Intergovernmental Panel on Climate Change. Cambridge University Press, Cambridge, United Kingdom and New York, NY, USA, pp. 1137–1216.

Cooper, M.J., Beevers, M.D., Oppenheimer, M., 2008. The potential impacts of sea level rise on the coastal region of New Jersey, USA. Clim. Change 90 (4), 475–492. https://doi.org/10.1007/s10584-008-9422-0.

Cutter, S.L., 1996. Vulnerability to environmental hazards. Prog. Hum. Geogr. 20 (4), 529–539.

Denner, K., Phillips, M.R., Jenkins, R.E., Thomas, T., 2015. A coastal vulnerability and environmental risk assessment of Loughor Estuary, South Wales. Ocean Coast. Manag. 116, 478–490. https://doi.org/10.1016/j.ocecoaman.2015.09.002.

Dewi, R.S., Bijker, W., Stein, A., Marfai, M.A., 2016. Fuzzy classification for shoreline change monitoring in a part of the Northern Coastal Area of Java, Indonesia. Remote Sens. 8 (3), 190. https://doi.org/10.3390/rs8030190.

Di Paola, G. et al., 2011. Estimating coastal vulnerability in a meso-tidal beach by means of quantitative and semi-quantitative methodologies. J. Coastal Res. 61, 303–308. https://doi.org/10.2112/SI61-001.30.

Diez, P., Perillo, G., Piccolo, M., 2007. Vulnerability to sea-level rise on the coast of the Buenos Aires Province. J. Coast. Res. 23, 119–142.

Domínguez, L., Anfuso, G., Gracia, F., 2005. Vulnerability assessment of a retreating coast in SW Spain. Environ. Geol. 47, 1037–1044. https://doi.org/10.1007/s00254-005-1235-0.

Doukakis, E., 2005. Coastal vulnerability and risk parameters, s.l.: Eur. Water 11/12, 3e7.

Duriyapong, F., Nakhapakorn, K., 2011. Coastal vulnerability assessment: a case study of Samut Sakhon coastal zone. Songklanakarin J. Sci. Technol. 33 (4), 469–476.

EORC (JAXA Earth Observation Research Center), 2008. ALOS data users handbook-revision C. Earth Observation Research and Application Center Japan Aerospace Exploration Agency. Available at: <http://www.eorc.jaxa.jp/ALOS/en/doc/fdata/ALOS_HB_RevC_EN.pdf>.

Farhan, A.R., Lim, S., 2012. Vulnerability assessment of ecological conditions in Seribu Islands, Indonesia. Ocean Coastal Manag. 65, 1–14. https://doi.org/10.1016/j.ocecoaman.2012.04.015.

Ferretti, A., et al., 2015. InSAR data for monitoring land subsidence: time to think big. 372, 331. s.l., s.n., p. 372. <https://doi.org/10.5194/piahs-372-331-2015>.

Firman, T., 2007. The urbanisation of Java, 2000–2010: towards 'the island of mega-urban regions'. Asian Popul. Stud. 13 (1), 50–66. https://doi.org/10.1080/17441730.2016.1247587.

Fitzpatrick-Lins, K., 1981. Comparison of sampling procedures and data analysis for a land-use and land-cover map. Photogramm. Eng. Remote Sens. 47 (3), 343–351.

Gaffara, G., Hisbaron, D.R., Marfai, M., 2017. Land use changes analysis for land subsidence in coastal areas (Case Study: North Semarang District). Indonesian J. Geogr. 19 (2), 121–134. https://doi.org/10.1080/19475705.2012.692336.

Gaki-Papanastassiou, K. et al., 2010. Coastal vulnerability assessment to sea-level rise based on geomorphological and oceanographical parameters: the case of Argolikos Gulf, Peloponnese, Greece. Hellenic J. Geosci. 45 (45), 109–122.

Goldstein, R.M., Wenner, C.L., 1998. Radar interferogram filtering for geophysical applications. Geophys. Res. Lett. 25 (21), 4035–4038.

Gornitz, V., White, T., Cushman, R., 1991. Vulnerability of the U.S. to future sea-level rise. Long Beach, s.n., pp. 2354–2368.

Gornitz, V., 1990. Vulnerability of the East Coast, USA to future sea level rise. J. Coastal Res. 9, 201–237.

Gornitz, V.M., Daniels, R.C., White, T.W., Birdwell, K.R., 1994. The development of a coastal risk assessment database: vulnerability to sea-level rise in the US Southeast. J. Coastal Res., 327–338

Gornitz V.M., White T.W., 1992. A coastal hazard data base for the U.S. East Coast, The University of Tennessee; Tennessee.

Hadi, F., et al., 2016. Urban growth and land use/land cover modeling in Semarang, Central Java, Indonesia. Colombo-Srilanka, ACRS2016.

Handayani, W., Rudiarto, I., 2014. Dynamics of urban growth in semarang metropolitan-central java: an examination based on built-up area and population change. J. Geogr. Geol. 6 (4), 80–87. https://doi.org/10.5539/jgg.v6n4p80.

Harwitasari, D., Van Ast, J.A., 2011. Climate change adaptation in practice: people's responses to tidal flooding in Semarang, Indonesia. J. Flood Risk Manag. 4 (3), 216–233. https://doi.org/10.1111/j.1753-318X.2011.01104.x.

Kasim, F., Siregar, V.P., 2012. Coastal vulnerability assessment using integrated method of CVI-MCA: a case study on the coastline of Indramayu. Geogr. Forum 26, 65–76.

Klein, R.J., Nicholls, R.J., 1999. Assessment of coastal vulnerability to climate change. Ambio, 182–187.

Klemas, V., 2010. Remote sensing techniques for studying coastal ecosystems: an overview. J. Coastal Res. 27 (1), 2–17. https://doi.org/10.2112/JCOASTRES-D-10-00103.1.

Kumar, A.A., Kunte, P.D., 2012. Coastal vulnerability assessment for Chennai, east coast of India using geospatial techniques. Nat. Hazards 64 (1), 853–872. https://doi.org/10.1007/s11069-012-0276-4.

Kumar, T.S. et al., 2010. Coastal vulnerability assessment for Orissa State, East coast of India. J. Coastal Res. 26 (3), 523–534. https://doi.org/10.2112/09-1186.1.

Kunte, P.D. et al., 2014. Multi-hazards coastal vulnerability assessment of Goa, India, Using geospatial techniques. Ocean Coastal Manag. 95, 264–281. https://doi.org/10.1016/j.ocecoaman.2014.04.024.

Li, Y. et al., 2016. Assessing spatial vulnerability from rapid urbanization to inform coastal urban regional planning. Ocean Coast. Manag. 123, 53–65. https://doi.org/10.1016/j.ocecoaman.2016.01.010.

Lillesand, T.M., Kiefer, R.W., 2000. Remote Sensing and Image Interpretation. John Wiley & Sons, New York.

Lubis, A.M. et al., 2011. Ground subsidence in Semarang-Indonesia investigated by ALOS–PALSAR satellite SAR interferometry. J. Asian Earth Sci. 40 (5), 1079–1088. https://doi.org/10.1016/j.jseaes.2010.12.001.

Mahapatra, M., Ramakrishnan, R., Rajawat, A.S., 2015. Coastal vulnerability assessment of Gujarat coast to sea level rise using GIS techniques: a preliminary study. J. Coast Conserv. 19 (2), 241–256. https://doi.org/10.1007/s11852-015-0384-x.

Marfai, M.A., 2011. The hazards of coastal erosion in Central Java, Indonesia: an overview. Geografia-Malaysian J. Soc. Space 7 (3), 1–9.

Marfai, M.A. et al., 2008. Coastal dynamic and shoreline mapping: multi-sources spatial data analysis in Semarang Indonesia. Environ. Monitor. Assess. 142 (2), 297–308.

Marfai, M.A., King, L., 2007. Monitoring land subsidence in Semarang, Indonesia. Environ. Geol. 53 (3), 651–659. https://doi.org/10.1007/s00254-007-0680-3.

Marfai, M.A., King, L., 2008. Potential vulnerability implications of coastal inundation due to sea level rise for the coastal zone of Semarang city, Indonesia. Environ. Geol. 54 (6), 1235–1245. https://doi.org/10.1007/s00254-007-0906-4.

Martins, K., Souza Pereira, P.D., Silva-Casarín, R., Nogueira Neto, A.V., 2017. The influence of climate change on coastal erosion vulnerability in northeast Brazil. Coastal Eng. J. 59 (2), 1740007. https://doi.org/10.1142/S0578563417400071.

McGranahan, G., Balk, D., Anderson, B., 2007. The rising tide: assessing the risks of climate change and human settlements in low elevation coastal zones. Environ. Urban. 19 (1), 17–37.

Meilistya, I., Sugianto, D.N., Indrayanti, E., 2012. Kajian Arus Sejajar Pantai (Longshore Current) Akibat Pengaruh Transformasi Gelombang Di Perairan Semarang (in Bahasa). J. Oceanogr. 1 (2), 128–138.

NBDC and NOAA. 2017. At: <http://www.ndbc.noaa.gov/measdes.shtml>.

Nguyen, T.T., Bonetti, J., Rogers, K., Woodroffe, C.D., 2016. Indicator-based assessment of climate-change impacts on coasts: a review of concepts, methodological approaches and vulnerability indices. Ocean Coast. Manag. 123, 18–43. https://doi.org/10.1016/j.ocecoaman.2015.11.022.

Nicholls, R.J., 1995. Coastal megacities and climate change. GeoJournal 37 (3), 369–379. https://doi.org/10.1007/BF00814018.

Palmer, B.J. et al., 2011. Preliminary coastal vulnerability assessment for KwaZulu-Natal, South Africa. J. Coastal Res. 64, 1390.

Pendleton, E. A., Barras, J. & Williams, S., 2010. Coastal vulnerability assessment of the Northern Gulf of Mexico to sea-level rise and coastal change: U.S, U.S.: Geological Survey Open-File Report.

Pendleton, E.A., Thieler, E.R., Williams, S.J., 2005. Coastal vulnerability assessment of golden gate national recreation area to sea level rise-Open-File Report 2005–1058. US Geological Survey, Reston, Virginia.

Qu, F. et al., 2014. Land subsidence and ground fissures in Xi'an, China 2005–2012 revealed by multi-band InSAR time-series analysis. Remote Sens. Environ. 155, 366–376. https://doi.org/10.1016/j.rse.2014.09.008.

Rahmawati, N., Vuillaume, J.F., Purnama, I.L.S., 2013. Salt intrusion in Coastal and Lowland areas of Semarang City. J. Hydrol. 494, 146–159. https://doi.org/10.1016/j.jhydrol.2013.04.031.

Ramieri, E. et al., 2011. Methods for assessing coastal vulnerability to climate change. European Topic Centre on climate change impacts, vulnerability and adaptation, Bologna, Italy.: (ETC CCA) technical paper.

Rao, K.N. et al., 2008. Sea-level rise and coastal vulnerability: an assessment of Andhra Pradesh coast, India through remote sensing and GIS. J. Coastal Conserv. 12 (4), 195–207. https://doi.org/10.1007/s11852-009-0042-2.

Rocca, F., Prati, C., Guarnieri, M., Ferretti, A., 2000. SAR interferometry and its application. Surveys Geophys. 21, 159–176. https://doi.org/10.1023/A:1006710731155.

Sandwell, D. et al., 2014. GMTSAR: An InSAR Processing System Based on Generic Mapping Tools. Scripps Institution of Oceanography University of California, San Diego.

Shanas, P.R., Kumar, V.S., 2014. Trends in surface wind speed and significant wave height as revealed by ERA-Interim wind wave hindcast in the Central Bay of Bengal. Int. J. Climatol. 35 (9), 2654–2663.

Semarang, 2014. Pemerintah Kota Semarang (in Bahasa). Available at: <http://semarangkota.go.id/main/page/2/profil> (accessed 10 2 2017).

Sun, H. et al., 2017. Monitoring land subsidence in the southern part of the lower Liaohe plain, China with a multi-track PS-InSAR technique. Remote Sens. Environ. 188, 73–84. https://doi.org/10.1016/j.rse.2016.10.037.

Thieler,. E. & Hammar-Klose, E., 1999. National Assessment of Coastal Vulnerability to Future Sea-level Rise: Preliminary Results for the U.S., Atlantic Coast. U.S.: Geological Survey, pp. 99e593. Open-File Report.

Thieler, E.R., Hammar-Klose, E.S., 2000. National Assessment of Coastal Vulnerability to Sea-Level Rise: Preliminary Results for the U.S. Pacific Coast, Woods Hole, Mass, USA, s.n.

Turner, R.K. et al., 2004. An ecological economics approach to the management of a multi-purpose coastal wetland. 4(2–3). Reg. Environ. Change 4 (2–3), 86–99. https://doi.org/10.1007/s10113-004-0075-x.

Tyo, J.S., Goldstein, D.L., Chenault, D.B., Shaw, J.A., 2006. Review of passive imaging polarimetry for remote sensing applications. Appl. Opt. 45 (22), 5453–5469.

Wang, J., Gao, W., Xu, S., Yu, L., 2012. Evaluation of the combined risk of sea level rise, land subsidence, and storm surges on the coastal areas of Shanghai, China. Climatic Change 115 (3–4), 537–558. https://doi.org/10.1007/s10584-012-0468-7.

Wöppelmann, G. et al., 2013. Is land subsidence increasing the exposure to sea level rise in Alexandria, Egypt? Geophys. Res. Lett. 40 (12), 2953–2957. https://doi.org/10.1002/grl.50568.

Wu, S.Y., Yarnal, B., Fisher, A., 2002. Vulnerability of coastal communities to sea-level rise: a case study of Cape May County, New Jersey, USA. Climate Res. 22 (3), 255–270. https://doi.org/10.3354/cr022255.

Yeung, Y.M., 2001. Coastal mega-cities in Asia: transformation, sustainability and management. Ocean Coast. Manag. 44 (5), 319–333. https://doi.org/10.1016/S0964-5691(01)00053-9.

Yin, J., Yin, Z., Wang, J., Xu, S., 2012. National assessment of coastal vulnerability to sea-level rise for the Chinese coast. J. Coastal Conserv. 16 (1), 123–133.

ORIGINALITY REPORT

13% SIMILARITY INDEX

13% INTERNET SOURCES

11% PUBLICATIONS

8% STUDENT PAPERS

PRIMARY SOURCES

1. Rakesh Bera, Ramkrishna Maiti. "An assessment of coastal vulnerability using geospatial techniques", Environmental Earth Sciences, 2021
   Publication
   5%

2. www.science.gov
   Internet Source
   3%

3. research-information.bris.ac.uk
   Internet Source
   1%

4. link.springer.com
   Internet Source
   1%

5. www.int-arch-photogramm-remote-sens-spatial-inf-sci.net
   Internet Source
   1%

6. Submitted to University of KwaZulu-Natal
   Student Paper
   1%

7. Pravin D. Kunte, Nitesh Jauhari, Utkarsh Mehrotra, Mahender Kotha, Andrew S. Hursthouse, Alexandre S. Gagnon. "Multi-hazards coastal vulnerability assessment of
   1%

Goa, India, using geospatial techniques",
Ocean & Coastal Management, 2014
Publication

8	www.e3s-conferences.org	1 %
	Internet Source	

Exclude quotes   Off   Exclude matches   < 1%
Exclude bibliography   On